IEEE Access
Multidisciplinary | Rapid Review | Open Access Journal

Received 26 April 2025, accepted 22 May 2025, date of publication 2 June 2025, date of current version 9 June 2025.

Digital Object Identifier 10.1109/ACCESS.2025.3575932

RESEARCH ARTICLE

Accurate Radar-Based Heartbeat Measurement Using Higher Harmonic Components

ITSUKI IWATA[1], KIMITAKA SUMI[1], (Graduate Student Member, IEEE), YUJI TANAKA[2], (Member, IEEE), AND TAKUYA SAKAMOTO[1], (Senior Member, IEEE)

[1]Department of Electrical Engineering, Graduate School of Engineering, Kyoto University, Kyoto 615-8510, Japan
[2]Graduate School of Engineering, Nagoya Institute of Technology, Nagoya 466-8555, Japan

Corresponding author: Takuya Sakamoto (sakamoto.takuya.8n@kyoto-u.ac.jp)

This work was supported in part by the SECOM Science and Technology Foundation; in part by Japan Science and Technology Agency under Grant JPMJMI22J2 and Grant JPMJMS2296; in part by Japan Society for the Promotion of Science KAKENHI under Grant 19H02155, Grant 21H03427, Grant 23H01420, Grant 23K19119, Grant 23K26115, and Grant 24K17286; and in part by the Terumo Life Science Foundation.

This work involved human subjects or animals in its research. Approval of all ethical and experimental procedures and protocols was granted by the Ethics Committee of the Graduate School of Engineering, Kyoto University, under Application Nos. 201916, 202214, and 202223.

ABSTRACT This study proposes a radar-based heartbeat measurement method that uses the absolute value of the second derivative of the complex radar signal, rather than its phase, in combination with the variational mode extraction method, which is a type of mode decomposition algorithm. We show that the proposed second-derivative-based approach can amplify the heartbeat component in the radar signals effectively. We also confirm that the use of the variational mode extraction method provides an efficient way to emphasize the heartbeat component when amplified via the second-derivative-based approach. We then demonstrate estimation of the interbeat intervals of the heart by using the proposed approach in combination with the topology method, which is an accurate interbeat interval estimation method. The performance of the proposed method is quantitatively evaluated using data acquired from eleven participants that were measured using a millimeter-wave radar system. Compared with the conventional methods based on the phase of the complex radar signal, our proposed method can achieve higher precision when estimating the heart's interbeat intervals; the correlation coefficient for the proposed method was increased by 0.20 and the root mean square error was reduced by 23%.

INDEX TERMS Displacement signal, FMCW radar, harmonic analysis, heart rate, interbeat interval, topology method, variational mode extraction.

I. INTRODUCTION

Radar-based technology for physiological signal measurement is expected to change the entire concept of health management because this technology can enable continuous monitoring of the health and the mental status of patients who are visible within a scene. Currently, physiological measurements for healthcare applications are based on the use of contact-type sensors, including electrocardiogram sensors with electrodes, pulse oximeter devices based on optical sensors, and blood pressure monitors that require a cuff to be wrapped around the patient's arm. The use of contact-type sensors to perform continuous long-term measurements can cause discomfort for the user or may impose restrictions on their activities [1], [2], but these problems can be avoided by introducing noncontact radar-based measurement technology [3].

Radar-based measurements of physiological signals use radar echoes that are reflected by the surface of the human body and modulated by the body's displacements. The heartbeat causes a semiperiodic displacement that can be observed throughout the human body [4] and the displacement caused

The associate editor coordinating the review of this manuscript and approving it for publication was Patrizia Livreri.

by the heartbeat can be expressed as a sum of the motion of the heart and the volumetric changes in the pulse waves that propagate through the arteries. In principle, by estimating the power spectrum of these displacements, we are then able to detect the respiratory and heartbeat components within the frequency domain. Because these respiratory and heartbeat components are semiperiodic but are not sinusoidal, they also contain higher-order harmonics in addition to their fundamental frequencies [5], [6].

A typical respiratory displacement has a fundamental frequency between 0.1 and 0.3 Hz and a displacement magnitude between 4 and 12 mm, whereas a typical heartbeat displacement has a fundamental frequency between 1 and 1.7 Hz, with a displacement magnitude between 0.2 and 0.5 mm [7], [8], [9]. It is often difficult to identify the fundamental frequency of the heartbeat in the frequency domain because this fundamental frequency component can be masked by the higher-order harmonic components of the respiration. Therefore, a sophisticated approach is required to estimate the heartbeat component within the frequency domain, particularly when it is necessary to estimate the heart rate variability (HRV) or the interbeat intervals (IBIs) of the heart [4], [6], [10], [11], [12]. For example, Yamamoto et al. [13], [14] extracted the heartbeat component signal from radar data using a bandpass filter and then used a convolutional long short-term memory (LSTM) algorithm to estimate the IBIs. In addition, Wang et al. [15], [16] extracted the heartbeat component signal from radar data using a variational mode decomposition (VMD) approach. Petrović et al. [1] applied a bandpass filter to a complex radar signal using filter parameters that were set beforehand using a roughly estimated heart rate; this was followed by the application of a filter bank with narrow band-pass filters and resulted in IBI estimation using the zero-crossing points.

Although these methods have estimated the heartbeat parameters by focusing on the fundamental heartbeat frequency, the accuracy of their estimation is dependent on the intensity of the heartbeat's fundamental frequency component, which can easily be masked by the respiratory components. To overcome this issue, some existing studies focused on the harmonic frequency components of the heartbeat, rather than the fundamental frequency [1], [10], [11], [17]. Rong and Bliss [11] reported that the second harmonic component of the heartbeat is significantly greater than the higher-order respiratory harmonics. In addition, Petrović et al. [1] showed that the heartbeat's higher harmonics are much larger than the higher respiratory harmonics within the high-frequency band. Therefore, it is advantageous to use these higher harmonics to extract the heartbeat parameters instead of the fundamental component. Furthermore, the use of the second harmonic component of the heartbeat has been reported to be effective in suppressing the respiratory components [10], [18]. Iwata et al. [19] extracted the second harmonic component of the heartbeat signal to adjust their filter parameters to ensure that they emphasized the heartbeat component.

To emphasize the heartbeat's higher harmonics while also suppressing the respiratory components, it is necessary to use signal processing methods such as the application of a high-pass filter. To form the required high-pass filter, some studies have used the time derivative of the displacement waveform that can be estimated based on the phase of the complex radar signal [5], [12], [20], [21], [22], [23]. To explain these methods, let us assume here that $s(t)$ is a complex radar signal in the time domain. Wang et al. [5] suppressed the higher respiratory harmonics in the signal by introducing the first derivative of the radar signal phase (i.e., $(\mathrm{d}/\mathrm{d}t)\angle s(t)$). Kakouche et al. [20] also used the first derivative of the radar signal phase ($(\mathrm{d}/\mathrm{d}t)\angle s(t)$) when they applied the delay-and-sum method in the frequency domain. Yen et al. [21] also emphasized the heartbeat component by using $(\mathrm{d}/\mathrm{d}t)\angle s(t)$. In contrast, Xiong et al. [22] and Ji et al. [23] both emphasized the higher harmonics of the heartbeat by using a differential enhancement method that combined the first derivative (i.e., $(\mathrm{d}/\mathrm{d}t)\angle s(t)$) with the second derivative (i.e., $(\mathrm{d}^2/\mathrm{d}t^2)\angle s(t)$) of the phase of the radar signal. Nosrati and Tavassolian [12] used the second derivative of a complex radar signal (that is, $(\mathrm{d}^2/\mathrm{d}t^2)s(t)$) to emphasize the heartbeat component in a method in which the complex signal is used, rather than its phase. Sakamoto and Yamaguchi [24] used the absolute value of the second derivative of the complex radar signal (i.e., they used $|(\mathrm{d}^2/\mathrm{d}t^2)s(t)|$) to estimate the accuracy when measuring the heart rate.

In this study, we demonstrate the effectiveness of using the absolute value of the second derivative of the complex radar signal, as previously proposed in [12] and [24], when focusing on the higher harmonics of the heartbeat signal to estimate the heart rate. The advantage of this approach is that the method is independent of the phase-demodulation accuracy because the complex signal itself is used directly in the estimation process. This study also introduces the variational mode extraction (VME) process, which is a mode decomposition method, to further amplify the heartbeat component emphasized by the differentiation process. The performance of the proposed method is quantitatively evaluated by conducting radar measurement experiments involving eleven participants. In addition, we examine the performance of the proposed method under various conditions in terms of distance, angle, and height, and we also compare the calculation times for the conventional and proposed methods. A preprint of this manuscript has been posted online [25].

II. RADAR MEASUREMENT OF PHYSIOLOGICAL SIGNALS

A. RADAR IMAGING AND ESTIMATION OF BODY DISPLACEMENT

In this section, we use a 79 GHz frequency-modulated continuous-wave (FMCW) radar system with array antennas. When we use the FMCW demodulation method, the signal received using the mth element (or virtual element) is denoted by $s_m(r, t)$ ($m = 1, 2, \cdots, M$), where r and t represent the range and the slow time, respectively. Assuming that an M-

element linear array with spacing of $\lambda/2$ is used, we obtain a complex radar image that is defined by $I'_{\mathrm{C}}(r,\theta,t) = \sum_{m=1}^{M} \mathrm{e}^{\mathrm{j}\pi m \sin\theta} s_m(r,t)$, where λ and θ denote the wavelength and the azimuth angle, respectively. To remove any stationary clutter, the time average is subtracted from $I'_{\mathrm{C}}(r,\theta,t)$ as $I_{\mathrm{C}}(r,\theta,t) = I'_{\mathrm{C}}(r,\theta,t) - (1/T)\int_0^T I'_{\mathrm{C}}(r,\theta,t)\mathrm{d}t$ to generate $I_{\mathrm{C}}(r,\theta,t)$, where T is the measurement time. We then generate a power radar image $I_{\mathrm{P}} = |I_{\mathrm{C}}|^2$, which is time-averaged to produce the time-averaged power radar image $I_{\mathrm{A}}(r,\theta) = (1/T)\int_0^T I_{\mathrm{P}}(r,\theta,t)\mathrm{d}t$. The target position (r_0,θ_0) for the estimation of physiological signals is then determined using $I_{\mathrm{A}}(r,\theta)$, and we obtain the complex radar signal $s(t) = I_{\mathrm{C}}(r_0,\theta_0,t)$ and the body displacement $d(t)$, where $d(t) = (\lambda/4\pi)\angle s(t)$ and $\angle$ denotes the phase of a complex number.

B. MODE DECOMPOSITION METHODS

Mode decomposition, which is a type of mix source separation method, can decompose an input signal into multiple components and subsequently reconstruct the signal by simply selecting the desired mode [26], [27]. Therefore, it is anticipated that application of mode decomposition to the proposed signal $|s''(t)|$ will cause the heartbeat harmonic components to be enhanced, thus leading to improved accuracy when estimating IBIs. Mode decomposition has previously been applied to the phase $\psi(t)$ or displacement $d(t)$ to estimate the respiration and heartbeat parameters [28], [29], [30], [31], [32].

VMD [16], which is a type of mix source separation method, was developed by Dragomiretskiy and Zosso in 2014. In VMD, the intrinsic mode function (IMF) is defined as an amplitude- and frequency-modulated signal:

$$u_k(t) = A_k(t)\cos(\phi_k(t)), \tag{1}$$

where $k = 1,\ldots,K_{\mathrm{v}}$ and K_{v} is the number of modes. The phase $\phi_k(t)$ is a nondecreasing function, which means that $\phi'_k(t) = (\mathrm{d}/\mathrm{d}t)\phi_k(t) \geq 0$. The envelope $A_k(t) \geq 0$ and both $A_k(t)$ and the instantaneous frequency $\phi'_k(t)$ vary sufficiently slowly to ensure that, over a sufficiently long time $[t - t_0, t + t_0]$ (where $t_0 \geq 2\pi/\phi'_k(t)$), $u_k(t)$ can be regarded as a pure harmonic signal with amplitude $A_k(t)$ and instantaneous frequency $\phi'_k(t)$. Therefore, the IMF has a specific sparsity property [16]. In VMD, it is assumed that each IMF u_k is located around the kth central frequency f_k. Determining the pairing of u_k and f_k that minimizes the constrained variational problem allows the input signal with the real value to be decomposed into each mode.

The VMD is superior to empirical mode decomposition (EMD) methods in terms of both IMF separation and noise robustness [33]. As a result of its high performance, VMD has been widely used in radar measurements of physiological signals [5], [15], [18], [34], [35], [36]. Lele et al. reconstructed both respiratory and heartbeat signals by summing IMFs that satisfied a threshold ratio condition between the total energy of each IMF in the frequency domain and the energy contained within the fundamental frequency ranges of the respiration and heartbeat signals only [37]. However, the performance of VMD depends on both the number of decomposition layers K_{v} used and the penalty coefficient α [16], [38]. A low α value can lead to reduced decomposition accuracy due to noise since the value of α affects the bandwidth of each decomposed component. The number of decomposition layers K_{v} used also affects the decomposition results; a small K_{v} value, which means fewer IMFs, can lead to mode mixing. A large K_{v} value can lead to the overlap of the central frequencies, the decomposition of signals into more than two IMFs, and a reduction in the accuracy of the mode decomposition.

In this study, we use VME [39], a VMD-based method proposed by Nazari and Sakhaei, to enable effective extraction of the harmonic components of the heartbeat. The VME algorithm is shown in concise form in Algorithm 1. The VME method was developed from the VMD to extract respiratory signals from electrocardiograph (ECG) signals [39]. In VME, the desired mode $u_{\mathrm{d}}(t)$ and the residual $r_{\mathrm{d}}(t)$ are defined, and a penalty term is then added to the VMD objective function to define the optimization problem, as follows:

$$\min_{u_{\mathrm{d}},\,\omega_{\mathrm{d}},\,r_{\mathrm{d}}} \left\{\alpha B_{\mathrm{d}}^2 + \|\beta(t) * r_{\mathrm{d}}(t)\|_2^2\right\} \tag{2}$$

$$\text{s. t.}\quad u_{\mathrm{d}}(t) + r_{\mathrm{d}}(t) = |s''(t)|, \tag{3}$$

where the penalty coefficient α is a parameter that balances the first and second terms of the objective function, and B_{d} is the bandwidth of the desired mode and is expressed as

$$B_{\mathrm{d}} = \left\|\frac{\mathrm{d}}{\mathrm{d}t}\left[\left(\delta(t) + \frac{\mathrm{j}}{\pi t}\right) * u_{\mathrm{d}}(t)\right]\mathrm{e}^{-\mathrm{j}\omega_{\mathrm{d}}t}\right\|_2^2. \tag{4}$$

For example, if $u_{\mathrm{d}}(t)$ is expressed as $u_{\mathrm{d}}(t) = A(t)\mathrm{e}^{\mathrm{j}\omega_{\mathrm{d}}t}$ using the real amplitude $A(t)$, then B_{d} is written as $B_{\mathrm{d}} = |(\mathrm{d}/\mathrm{d}t)A(t)|^2 + \omega_{\mathrm{d}}^2|A(t)|^2$, which is the sum of two terms that are both determined by the amplitude and its time derivative, and it has a large value when the bandwidth of $A(t)$ is sufficiently large. Note here that $\beta(t)$ is the impulse response of a filter, which is given by

$$B(f) = \mathcal{F}\{\beta(t)\} = \frac{1}{4\pi^2\alpha(f - f_{\mathrm{d}})^2} \tag{5}$$

and this filter has infinite gain at $f = f_{\mathrm{d}}$, but it behaves like a Wiener filter at frequencies other than f_{d}. The bandwidth of the extracted mode $u_{\mathrm{d}}(t)$ is affected by the bandwidth of $B(f)$ and is determined by α. Although it is important to selecte the appropriate value of α when using VME, this process will form a part of our future research because it is outside the scope of this study.

Unlike VMD, which determines all modes from the input signal and then iteratively decomposes them into each mode, VME only extracts the specific mode $u_{\mathrm{d}}(t)$, which has an approximate known central frequency f_{d}. Therefore, compared with conventional VMD, VME has both a higher convergence rate and a lower computational load. In addition to these characteristics, the VME method is useful for applications in which specific modes are extracted because it

Algorithm 1 VME Algorithm

Initialize $\hat{u}_\mathrm{d}^1$, $\hat{\mu}^1$, $n \leftarrow 0$, and $\omega_\mathrm{d}^1 \leftarrow$ initial guess

repeat

$\quad n \leftarrow n+1$

$\quad$ 1) Update $\hat{u}_\mathrm{d}^1$ for all $\omega \geq 0$:

$$\hat{u}_\mathrm{d}^{n+1}(\omega) = \frac{\hat{f}(\omega)+\alpha^2\left(\omega-\omega_\mathrm{d}^{n+1}\right)^4\hat{u}_\mathrm{d}^n(\omega)+\hat{\mu}(\omega)/2}{\left[1+\alpha^2(\omega-\omega_\mathrm{d}^{n+1})^4\right]\left[1+2\alpha(\omega-\omega_\mathrm{d}^n)^2\right]}$$

$\quad$ 2) Update ω_d: $\omega_\mathrm{d}^{n+1} = \frac{\int_0^\infty \omega|\hat{u}_\mathrm{d}^{n+1}(\omega)|^2 \mathrm{d}\omega}{\int_0^\infty |\hat{u}_\mathrm{d}^{n+1}(\omega)|^2 \mathrm{d}\omega}$

$\quad$ 3) Dual ascent for all $\omega \geq 0$:

$$\hat{\mu}^{n+1} = \hat{\mu}^n + \tau\left[\frac{\hat{f}(\omega)-\hat{u}_\mathrm{d}^{n+1}(\omega)}{1+\alpha^2(\omega-\omega_\mathrm{d}^{n+1})^4}\right]$$

until convergence: $\frac{\|\hat{u}_\mathrm{d}^{n+1}-\hat{u}_\mathrm{d}^n\|_2^2}{\|\hat{u}_\mathrm{d}^n\|_2^2} < \epsilon$.

does not need to provide K_v [2], [39]. Please note that one of the main reasons VME is used instead of VMD in this study is that VME does not require that the number of modes K_v is known. Therefore, we do not use K_v hereafter in this article. Similar to VMD, VME is affected by the parameter α; if the value of α is too high, then modes with narrow bandwidths are obtained, thus leading to the generation of artifacts due to noise; if the value of α is too low, then it is possible that multiple modes will be mixed, thus leading to the issue where the desired signal is not recognized as a single mode. Although a method to optimize the VME parameters using a genetic algorithm was proposed by Zhang et al. [40], α is empirically determined in this study. In a later section, we will assess the performance of the proposed method when using different values of α to demonstrate how the selection of this parameter affects the overall accuracy of the results.

In summary, mode-decomposition algorithms (including VMD, VME, EMD, ensemble EMD (EEMD), complete EEMD with adaptive noise (CEEMDAN), and improved CEEMDAN (ICEEMDAN) [41] algorithms) are used to decompose a signal into simpler components called modes, where each mode represents a different frequency or pattern. VME achieves signal decomposition by minimizing a cost function in an iterative manner using Eqs. (2) and (3) to extract a specific mode $u_\mathrm{d}(t)$ with an angular frequency ω_d; this frequency is close to the angular frequency given by the initial estimate performed using $|s''(t)|$ that emphasized the high-frequency harmonic components of the heartbeat. Unlike the other mode-decomposition algorithms, VME extracts the desired mode directly by solving a constrained optimization problem and thus ensures better mode separation and improved noise resistance.

III. PROPOSED HEART RATE ESTIMATION METHOD

Although many previous studies have used the signal phase $\psi(t)$ or the displacement $d(t)$ to measure the heartbeat [27], [42], [43], the accuracy obtained is not necessarily satisfactory as a result of the interference that occurs with the respiratory components. In this study, we propose a method that uses the absolute value of the second derivative of the complex radar signal $|(\mathrm{d}^2/\mathrm{d}t^2)s(t)| = |s''(t)|$ instead of the displacement $\psi(t)$, as described in [12] and [24].

Here, we present examples of signals that have been processed using different methods to demonstrate the effectiveness of our proposed approach; radar signals that were measured from two participants (designated A and B) are used for this purpose. Details of the experiments are presented in Section IV. First, we consider the power spectrum of $\psi(t) = \mathrm{unwrap}\{\angle s(t)\}$, where unwrap is a phase unwrapping function. The power spectra of $\psi(t)$ for participants A and B are shown in Fig. 1 (b) and Fig. 2 (b), respectively. Please note that the displacement $d(t)$ can be estimated using $d(t) = (\lambda/4\pi)\psi(t)$ if the signal contains only a single echo that has been reflected from a target with a displacement that varies over time. The fundamental frequency and the second and third harmonics of the heartbeat that were obtained from the ECG are shown as blue dashed lines. In these figures, we see peaks that correspond to the fundamental and harmonic components of the heartbeat, along with some much larger peaks that correspond to the respiratory components. The accuracy of the estimation of the heart rate from $d(t)$ depends on the intensity and the frequency of both the heartbeat and respiration signals; as a result, the accuracy may be degraded in some cases.

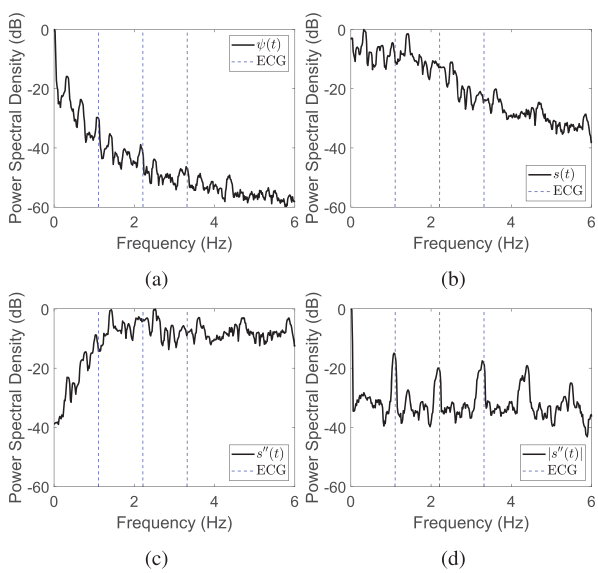

FIGURE 1. Participant A's Power spectral density functions for various forms of radar signal (black lines), along with the fundamental, second, and third harmonic frequencies of the heartbeat signal obtained from an ECG. (a) $|\mathcal{F}\{\psi(t)\}|^2$, (b) $|\mathcal{F}\{s(t)\}|^2$, (c) $|\mathcal{F}\{s''(t)\}|^2$, and (d) the proposed $|\mathcal{F}\{|s''(t)|\}|^2$.

Next, we consider the power spectrum of the complex radar signal $s(t)$ itself; the corresponding spectra for participants A and B are shown in Fig. 1 (b) and Fig. 2 (b), respectively. In these figures, the peaks that correspond to the heartbeat components are not shown clearly, which indicates that it is difficult to estimate the heart rate from $|\mathcal{F}\{s(t)\}|^2$, at least in part because of the interference from the respiratory harmonic components and the nonlinear effect of the phase modulation. Therefore, to emphasize the heartbeat harmonics at higher frequencies, we consider the power spectrum of the second derivative of the complex radar signal $s''(t)$; the corresponding spectra for participants A and B are shown in Fig. 1 (c) and Fig. 2 (c), respectively. Comparison of Fig. 1 (b) with Fig. 1 (c) and of Fig. 2 (b) with Fig. 2 (c) shows that the high-frequency components have been emphasized by the derivative operation. However, despite this emphasis, we are still unable to see clear peaks corresponding to the heartbeat components, even after the differentiation.

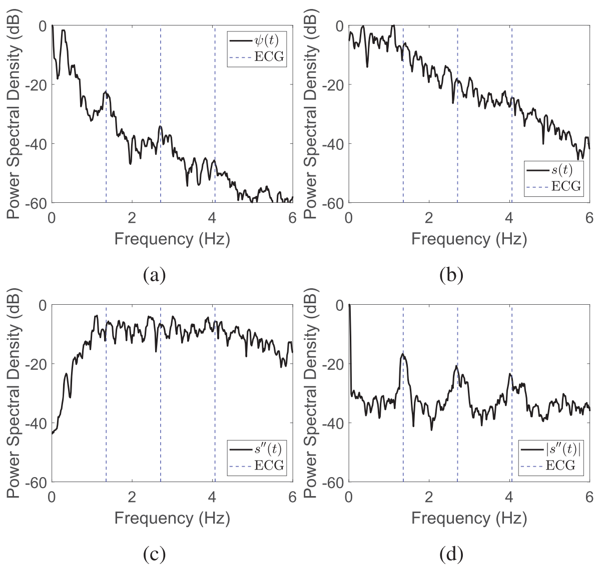

FIGURE 2. Participant B's power spectral density functions for various forms of radar signal (black lines), along with the fundamental, second, and third harmonic frequencies of the heartbeat signal obtained from an ECG. (a) $|\mathcal{F}\{\psi(t)\}|^2$, (b) $|\mathcal{F}\{s(t)\}|^2$, (c) $|\mathcal{F}\{s''(t)\}|^2$, and (d) the proposed $|\mathcal{F}\{|s''(t)|\}|^2$.

Figs. 1 (d) and 2 (d) show the characteristics of the power spectral density that correspond to $\mathcal{F}\{|s''(t)|\}$ for participants A and B, respectively. Comparison with Figs. 1 (b) and 2 (b) illustrates that Figs. 1 (d) and 2 (d) both show clear peaks that correspond to the fundamental and harmonic components of the heartbeat. Furthermore, a comparison of Fig. 1 (d) and Fig. 2 (d) with Fig. 1 (a) and Fig. 2 (a)shows that the heartbeat components, including their harmonic components, are emphasized in the former cases. These examples demonstrate the effectiveness of use of the absolute value of the second derivative of the complex radar signal $|s''(t)|$ when measuring heartbeat signals using radar.

Next, we discuss which of these terms contributes to this emphasis on the heartbeat components. For the complex radar signal $s(t)$ that is expressed as $s(t) = s_0(t)\mathrm{e}^{\mathrm{j}\psi(t)}$ and has an amplitude $s_0(t)$, which is an almost constant complex amplitude (i.e., $(\mathrm{d}/\mathrm{d}t)s_0(t) \simeq 0$), and a phase $\psi(t)$ that is a real function of t, the absolute value of its second derivative $|s''(t)|$ can be expressed as

$$\left|\frac{\mathrm{d}^2}{\mathrm{d}t^2}s(t)\right| \simeq |s_0(t)|\left|\left\{-\left(\frac{\mathrm{d}}{\mathrm{d}t}\psi(t)\right)^2+\mathrm{j}\frac{\mathrm{d}^2}{\mathrm{d}t^2}\psi(t)\right\}\mathrm{e}^{\mathrm{j}\psi(t)}\right| \tag{6}$$

$$= |s_0(t)|\sqrt{|\psi'(t)|^4+|\psi''(t)|^2}, \tag{7}$$

which comprises $\psi'(t)$ and $\psi''(t)$, which represent the first and second derivatives of the phase $\psi(t)$, respectively. We evaluate and compare the effectiveness of $\psi'(t)$ and $\psi''(t)$ as follows; by substituting $\psi''(t) = 0$ into Eq. (7), we obtain $|s''_1(t)| = |s_0(t)| \cdot |\psi'(t)|^2$; and substitution of $\psi'(t) = 0$ into Eq. (7) gives $|s''_2(t)| = |s_0(t)| \cdot |\psi''(t)|$. The power spectra of $|s''_1(t)|$ and $|s''_2(t)|$ are shown in Fig. 3 (a) and 3 (b) for participant A and are shown in Fig. 4 (a) and 4 (b) for participant B, respectively. Please note that in these power spectra, $s_0(t)$ is a function of time and is thus dependent on t, unlike the case in Eq. (7). These figures show that the heartbeat component is emphasized in the case of $|s''_2(t)|$ in particular because it contains the second derivative of the phase $\psi''(t)$.

Furthermore, when the power spectra of $|s''_2(t)|$ shown in Figs. 3 (b) and 4 (b) are compared with the results for the proposed $|s''(t)|$ in Figs. 1 (d) and 2 (d), we can see that the proposed approach is more effective than the use of $|s''_2(t)|$, thus indicating the superior performance of the proposed approach. Another advantage of the proposed approach based on $|s''(t)|$ is that it allows the phase unwrapping process to be omitted. Given that the phase unwrapping does not work correctly when the signal is noisy, this advantage is crucial when the proposed method is applied in practice.

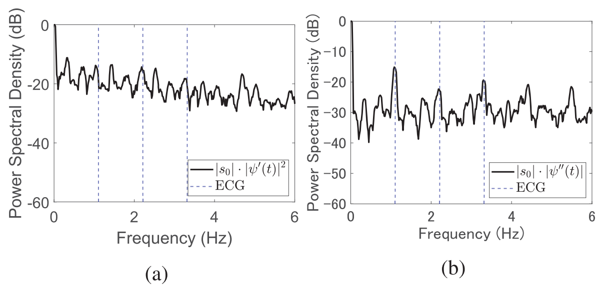

FIGURE 3. Participant A's power spectra for various forms of radar signal (black lines), along with the fundamental and second and third harmonic frequencies of the heartbeat signal obtained from an ECG; (a) $|s''_1(t)| = |s_0| \cdot |\psi'(t)|^2$ and (b) $|s''_2(t)| = |s_0| \cdot |\psi''(t)|$.

The power spectra given by

$$|\mathcal{F}\{|s^{(k)}(t)|\}|^2 = \left|\mathcal{F}\left\{\left|\frac{\mathrm{d}^k}{\mathrm{d}t^k}s(t)\right|\right\}\right|^2 \quad (k = 1, \ldots, 3) \tag{8}$$

for participant A are shown in Fig. 5 and those for participant B are shown in Fig. 6. Figs. 5 and 6 illustrate that the heartbeat component is emphasized most strongly for $k = 2$, thus justifying the use of our proposed approach with $|s''(t)|$.

Please note that Nosrati and Tavassolian [12] also examined the characteristics of $|\mathcal{F}\{s^{(k)}(t)\}|^2$ without taking the

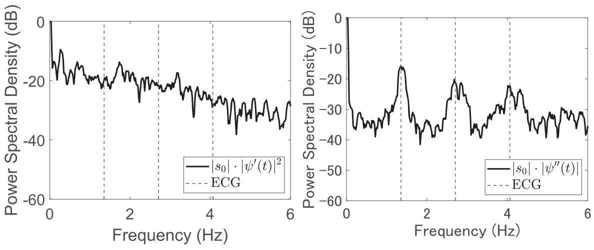

(a) (b)

FIGURE 4. Participant B's power spectra for various forms of radar signal (black lines), along with the fundamental and second and third harmonic frequencies of the heartbeat signal obtained from an ECG; (a) $|s''_1(t)| = |s_0| \cdot |\psi'(t)|^2$ and (b) $|s''_2(t)| = |s_0| \cdot |\psi''(t)|$.

absolute value, rather than use our proposed approach with $|\mathcal{F}\{|s^{(k)}(t)|\}|^2$, and they also demonstrated the effectiveness of differentiation for $k = 2$ among the other values of k. They also noted that when the order of differentiation increased, the harmonics of the respiration and the intermodulation waves of the respiration and the heartbeat were also amplified, which then reduced the signal-to-noise ratio (SNR) of the heartbeat component in addition to the numerical instability caused by the differentiation process. As they indicated, the heartbeat's SNR is expected to decrease when $k \geq 3$ because the noise in the higher frequency band is also emphasized by the differentiation operation. Therefore, we proposed the use of the absolute value of the second derivative $|s''(t)|$.

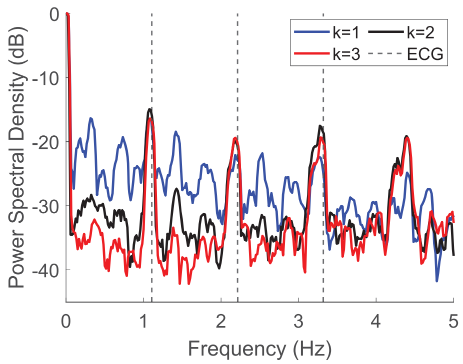

FIGURE 5. Participant A's power spectra $|\mathcal{F}\{|s^{(k)}(t)|\}|^2$, where the dashed lines indicate the fundamental and harmonic frequencies of the heartbeat.

The definitions used for the conventional and proposed methods are summarized in Table 1. The conventional methods all use $\psi(t)$, which represents the unwrapped phase of the complex radar signal, whereas the proposed methods all use $|s''(t)|$, which is the absolute value of the second derivative of the complex radar signal. Conventional method 1 and proposed method 1 do not apply VME. Conventional method 2 and proposed method 2 both apply ICEEMDAN [41] to extract the specific modes that contain a heartbeat component. ICEEMDAN has been widely used in radar-based physiological measurement applications [44], [45], [46]. Zhao et al. applied ICEEMDAN to body displacements measured using FMCW radar and reconstructed the corresponding heart rate signals by selecting the

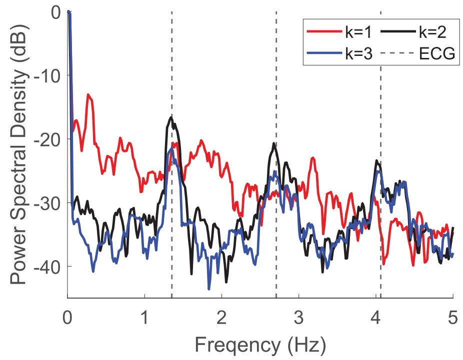

FIGURE 6. Participant B's power spectra $|\mathcal{F}\{|s^{(k)}(t)|\}|^2$, where the dashed lines indicate the fundamental and harmonic frequencies of the heartbeat.

appropriate IMF [44]. Hu and Toda identified the position of a moving participant and then applied ICEEMDAN to the displacements corresponding to the relevant coordinates to reconstruct the participant's respiratory and heart rate signals [45]. Yang and Bao used ICEEMDAN in combination with fast independent component analysis (Fast-ICA [47]) to suppress the harmonic components of the respiration signal and improve the SNR of the heart rate component [46]. Conventional method 3 and proposed method 3 both apply VME to extract the desired mode $u_\mathrm{d}(t)$ using the desired frequency f_d, which corresponds to the second harmonic frequency of the heartbeat signal. Here, f_d is selected as the frequency that corresponds to the maximum power spectrum density within the 2.0–3.4 Hz freuency range; i.e., $f_\mathrm{d} = \arg\max_f |\mathcal{F}\{|s''(t)|\}|^2$. Please note that if a local maximum point does not exist within this frequency range, we set $f_\mathrm{d} = 2.7$ Hz, which is the center frequency of the frequency range. Conventional method 4 and proposed method 4 follow the same steps used in conventional method 3 and proposed method 3, respectively, to extract $u_{\mathrm{d},1}(t)$; then, they apply the VME method again using the desired frequency $(3/2)f_\mathrm{d}$, which corresponds to the third harmonic frequency, extract the desired mode $u_{\mathrm{d},2}(t)$, and subsequently use the summation $u_{\mathrm{d},1}(t) + u_{\mathrm{d},2}(t)$. Conventional methods 1, 2, 3, and 4, and proposed methods 1, 2, 3, and 4 then all apply the topology method [48] to estimate the IBI. The VME parameter α is empirically set to have values of $\alpha = 10^5$ and $\alpha = 3 \times 10^4$ for the conventional and proposed methods, respectively.

TABLE 1. Conventional and proposed methods for IBI estimation.

Method	Signal to Process	Mode Decomposition	IBI Estimation
C1		—	
C2	$\psi(t)$	ICEEMDAN	Topology method
C3	$= \mathrm{unwrap}\{\angle s(t)\}$	VME mode 1	
C4		VME modes 1 & 2	
P1		—	
P2	$\left\lvert \frac{\mathrm{d}^2}{\mathrm{d}t^2} s(t) \right\rvert$	ICEEMDAN	Topology method
P3		VME mode 1	
P4		VME modes 1 & 2	

IV. PERFORMANCE EVALUATION OF THE PROPOSED METHODS

We used a 79 GHz millimeter-wave FMCW radar system with an antenna array composed of three transmitting elements and four receiving elements; the array specifications are listed in Table 2. The frame interval is 6.87 ms, which is the same value as the sampling interval in slow time; the number of chirp sets per frame is two; the chirp start frequency is 77.05 GHz; the ramp duration is 130 μs; the chirp frequency slope constant is 29.92 MHz/μs; the analog-to-digital converter (ADC) sampling frequency is 2.088 MHz; the number of ADC samples is 240; and the idle time between chirps is 150 μs. These parameters are illustrated in Fig. 7.

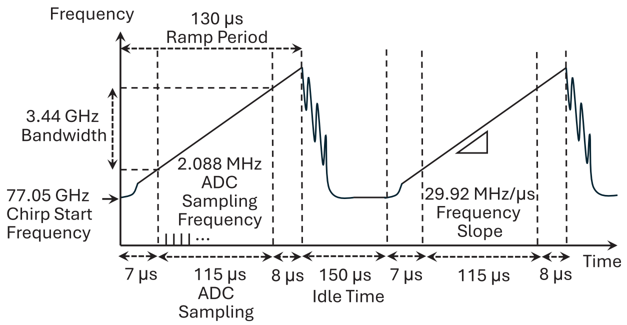

FIGURE 7. Chirp waveform parameters of the radar system.

The intervals between the elements were 2λ and λ/2 for the transmitting and receiving elements, respectively. The radar system was located at a distance of 1.0 m from each participant. Radar measurements were performed on eleven participants, who were all healthy adults, and a total of 25 samples of these measurements were used to evaluate the corresponding performances of the conventional and proposed methods. All participants were seated and breathed naturally for 60.0 s; the experimental scene is shown in Fig. 8. An ECG sensor was attached to each participant to evaluate the accuracy of the estimation of the heart IBI.

The experimental protocol used was as follows:

1) Instruct the participant to take a seat and breathe normally.
2) Attach an ECG sensor to the participant's chest.
3) Synchronize the ECG and radar sensors.
4) Begin the ECG and radar measurements simultaneously.
5) Finish the measurements and remove the ECG sensor from the participant's chest.

The performance of each method is evaluated in terms of the correlation coefficient (CC) between the actual IBI ($h_0(t)$) and the estimated IBI ($h(t)$), as given by

$$\frac{\int_0^T h_0(t)h(t)\mathrm{d}t}{\sqrt{\int_0^T h_0^2(t)\mathrm{d}t}\sqrt{\int_0^T h^2(t)\mathrm{d}t}}, \tag{9}$$

and the root-mean-square error (RMSE), which is given by

$$\sqrt{\frac{1}{T}\int_0^T |h(t)-h_0(t)|^2\mathrm{d}t}. \tag{10}$$

TABLE 2. Specifications of the radar system.

	Specification	unit
Tx element spacing	7.6	mm
Output power (EIRP)*	23	dBm
Tx element beamwidth (azimuth/elevation)	±35 / ±4	deg/deg
Rx element spacing	1.9	mm
Rx element beamwidth (azimuth/elevation)	±35 / ±4	deg/deg
Frequency range	77.0 – 80.9	GHz
Sampling intervals	6.87	ms

* EIRP: Equivalent isotropically radiated power.

TABLE 3. Demographic and physical characteristics of the participants.

Participant	Age (years)	Gender	Height (cm)	Weight (kg)	Chest circumference (cm)
A	23	Male	167	60	90
B	22	Male	173	65	90
C	23	Male	172	59	80
D	22	Male	165	53	79
E	22	Male	176	75	87
F	22	Male	176	66	90
G	23	Male	170	70	90
H	22	Male	180	63	86
I	24	Male	170	58	81
J	23	Male	169	52	77
K	23	Male	172	64	94
Mean	22.64	-	171.82	62.27	85.82
SD	0.64	-	4.13	6.55	5.39

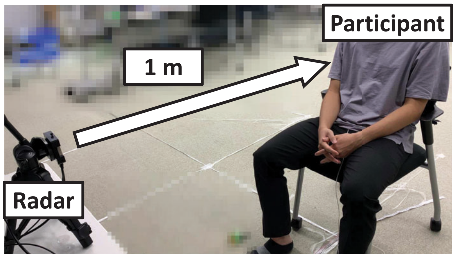

FIGURE 8. Experimental scene showing the measurement of a participant while breathing normally using millimeter-wave radar.

Performance is also evaluated in terms of the time coverage rate (TCR) [49]. The TCR is defined here as n/N, where N is the total number of time segments, which means that $N = T/T_0$, where T_0 is the time segment length; in addition, n is the number of time segments in which there is at least one IBI with an absolute error of less than T_{th} (that is, $\exists t \in T_n \quad |h(t) - h_0(t)| \le T_{\mathrm{th}}$ for $T_n = [nT_0, (n+1)T_0]$). We set these parameters empirically at $T_0 = 0.5$ s and $T_{\mathrm{th}} = 50$ ms. Please note that an accurate method is expected to achieve a high CC, a high TCR, and a low RMSE.

TABLE 4. IBI estimation evaluation index for each method.

	Method							
	C1	P1	C2	P2	C3	P3	C4	P4
CC	0.51	0.64	0.48	0.70	0.47	0.66	0.47	0.74
RMSE (ms)	47.07	33.42	39.61	28.80	37.03	31.44	34.42	26.02
TCR (%)	37.10	38.19	72.15	82.44	61.83	77.61	69.01	88.27

Table 4 shows the average values of the CC, RMSE, and TCR for each method, while Fig. 9 shows the average RMSE

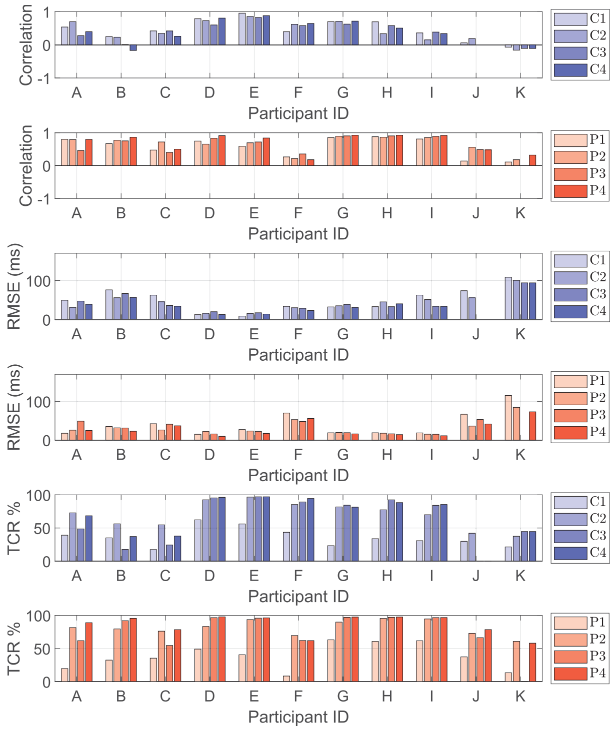

FIGURE 9. IBI estimation evaluation index characteristics for all participants.

and TCR values for the eleven participants. Comparison with proposed methods 1, 2, and 3 shows that proposed method 4 achieves the best improvement in terms of its CC, TCR, and RMSE values, thus indicating the effectiveness of the approach based on the extraction of the second and third heartbeat harmonics using VME. These results indicate that the topology method benefits from heartbeat harmonics of orders higher than three, rather than from the signals that contain only the second heartbeat harmonic component, and also they confirm that the use of $|s''(t)|$ enables greater accuracy to be achieved when compared with conventional methods using $\psi(t)$, which is proportional to the displacement $d(t)$. When the proposed method was used, the CC increased by 0.20, the RMSE decreased by 23%, and the TCR increased by 19% on average, which demonstes the effectiveness of the proposed method.

As an example, Fig. 10 shows the IBIs that were estimated using the conventional and proposed methods for participant A, where the CC, RMSE, and TCR values obtained were 0.15, 40.28 ms, and 77.50% when using the conventional method and 0.90, 11.76 ms and 96.67% when using the proposed method, respectively. Similarly, Fig. 11 shows the IBIs that were estimated using both the conventional and proposed methods for participant B, where the obtained CC, RMSE, and TCR values were −0.29, 71.67 ms and 51.26% when using the conventional method, and 0.93, 19.46 ms, and 94.96% when using the proposed method, respectively. By comparing Fig. 10 (a) with Fig. 10 (b) and also comparing Fig.11(a) with Fig. 11 (b), we see that the proposed methods can accurately estimate the IBIs over the entire measurement period. This performance improvement over the conventional methods can be attributed to the enhanced heartbeat components obtained.

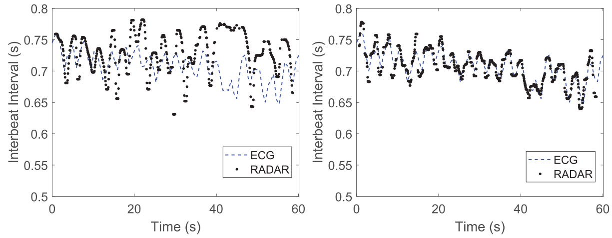

(a) (b)

FIGURE 10. Participant A's IBI as estimated using (a) conventional method 4 and (b) proposed method 4.

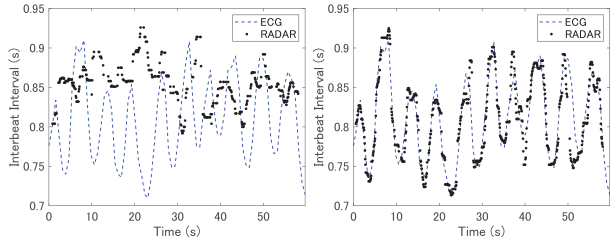

(a) (b)

FIGURE 11. Participant B's IBI as estimated using (a) conventional method 4 and (b) proposed method 4.

V. DISCUSSION

A. PERFORMANCE UNDER DIFFERENT CONDITIONS

Next, we investigated the performances of the conventional and proposed methods under a variety of experimental conditions. As shown in Table 5, experiments were conducted, during which we varied the target distance, the height of the radar, and the direction of the seats of the three participants (G, H and I) using the same scenarios that we described in Section IV. We applied conventional method 4 (C4) and proposed method 4 (P4), as described in Table 1.

TABLE 5. Experimental conditions variations.

Parameter	Condition	Distance (m)	Height (m)	Direction
Target distance	a_1	1.0	0.9	0°
	a_2	2.0		
	a_3	3.0		
Radar height	b_1	1.0	0.7	0°
	b_2		0.8	
	b_3		0.9	
Seating direction	c_1	1.0	0.9	0°
	c_2			45°
	c_3			90°
	c_4			135°
	c_5			180°

1) TARGET DISTANCE

As shown in Table 6, under the near-range condition (a_1), the proposed method P4 outperforms the conventional method C4, whereas under the mid-range and long-range conditions

(a_2 and a_3, respectively), the performance of proposed method P4 falls below that of the conventional method C4; this occurs partly because the SNR decreases when the target distance increases. Note also that the performance of conventional method C4 is not as sensitive to the target distance as proposed method P4. This result indicates that the proposed method is only effective when the SNR is sufficiently high.

TABLE 6. Performance for different target distances.

Condition	Method	RMSE (ms)	CC	TCR(%)
a_1	C4	35.14	0.52	85.05
	P4	13.72	0.92	97.21
a_2	C4	31.98	0.51	71.94
	P4	42.27	0.28	53.28
a_3	C4	30.75	0.50	68.27
	P4	45.19	0.29	52.15

2) RADAR HEIGHT

As shown in Table 7, proposed method P4 achieves high performance when the radar height is high and the radar antenna is facing the chest wall of the participant perpendicularly. This occurs because the line-of-sight displacement caused by the movement of the chest wall becomes greater as the radar height increases, which results in a higher SNR. In contrast, the performance of conventional method C4 does not improve significantly even when the SNR is high, partly because the performance degradation of the conventional method may mainly be caused by interference from the respiratory component rather than by noise.

TABLE 7. Performance at different radar heights.

Condition	Method	RMSE (ms)	CC	TCR(%)
b_1	C4	27.15	0.63	84.83
	P4	29.03	0.65	80.42
b_2	C4	33.32	0.48	61.63
	P4	25.07	0.71	78.42
b_3	C4	35.14	0.52	85.05
	P4	13.72	0.92	97.21

3) SEATING DIRECTION

The results in Table 8 show that the performance of conventional method C4 does not fluctuate much when the direction of the seat is changed, while proposed method P4 achieves its highest performance when the target participant faces the radar system directly. This result can also be explained by using the improvement that occurs in the SNR depending on the direction of the seat.

B. EXECUTION TIME EVALUATION

As an approximate indicator of computational complexity, we evaluated the average execution time (ET) for both the conventional methods and the proposed methods (Table 9).

TABLE 8. Performance for different seating directions.

Condition	Method	RMSE (ms)	CC	TCR (%)
c_1	C4	35.14	0.52	85.05
	P4	13.72	0.92	97.21
c_2	C4	29.01	0.56	47.31
	P4	46.41	0.30	55.80
c_3	C4	30.50	0.54	75.49
	P4	45.95	0.16	51.32
c_4	C4	46.69	0.11	36.02
	P4	30.18	0.61	75.26
c_5	C4	25.99	0.59	58.64
	P4	44.47	0.37	54.80

We evaluated the ET because VME is based on nonlinear optimization and the number of multiplication and addition operations is thus difficult to evaluate. To perform the evaluation, we used an Intel Xeon Gold 5218 central processing unit (CPU) (Intel Corporation, Santa Clara, CA, USA), 128 GB of main memory, and MATLAB R2024b software (MathWorks, Inc., Natick, MA, USA).

When the execution times for the conventional and proposed methods for each mode decomposition algorithm (e.g., C2 and P2) are compared, almost no significant differences are observed, except for those between C1 and P1. The reason for the increased execution time for P1 compared with that of C1 is that the topology method requires a longer execution time for a nonfiltered input signal $|s''(t)|$ that includes higher harmonic components without mode decomposition. In addition, the execution times for C2 and P2 are significantly longer than the corresponding times for the other methods as a result of the computational burden posed by ICEEMDAN. In contrast, the execution time for VME is much shorter than that required for ICEEMDAN.

TABLE 9. Average execution times for each method.

Method	Input	Mode Decomposition	ET (s)
C1	$\mathrm{unwrap}\{\angle s(t)\}$	—	3.77
C2		ICEEMDAN	30.09
C3		VME mode 1	0.27
C4		VME modes 1 & 2	0.53
P1	$\left\lvert\frac{\mathrm{d}^2}{\mathrm{d}t^2}s(t)\right\rvert$	—	10.97
P2		ICEEMDAN	30.57
P3		VME mode 1	0.23
P4		VME modes 1 & 2	0.44

C. PERFORMANCE FOR SECOND DERIVATIVE OF THE PHASE

Next, we evaluate the performance obtained when using the second derivative of phase $\psi''(t) = (\mathrm{d}^2/\mathrm{d}t^2)\mathrm{unwrap}\{\angle s(t)\}$ as the input. Table 10 presents the results for RMSE, CC, TCR, and ET that we obtained when the topology method was applied to $\psi''(t)$ and $|s''(t)|$ using VME modes 1 and 2, where we note that the case using $s''(t)$ corresponds to proposed method P4. From the table, we see that the performance obtained when using $\psi''(t)$ is not as high as that obtained when using $|s''(t)|$. In comparison to $\psi''(t)$, the performance of proposed method P4 was higher by 58.5% in terms of RMSE, by 0.58 points in terms of the CC, and 60% in terms of the TCR, although we did not observe any significant differences in terms of the ET. These results indicate that the use of $|s''(t)|$ is a key step to improve the accuracy of the IBI estimation.

TABLE 10. Comparison with second derivative of the phase.

Method	RMSE (ms)	CC	TCR (%)	ET (s)
$\psi''(t)$	62.75	0.16	28.91	0.46
$\|s''(t)\|$	26.02	0.74	88.27	0.44

D. PERFORMANCE FOR DIFFERENT VME PARAMETERS

We evaluated the performance of the proposed method when using different values of α, which affects the bandwidth of each decomposed component in the VME (Table 11). In the results presented in the table, we see that high performance was achieved when we set $\alpha = 100,000$. This occured in part because, for larger values of α, the bandwidth of each decomposed component becomes excessively narrow, and waveform distortion then occurs as a result; for small values of α, the bandwidth of each decomposed component becomes excessively broad, and a single decomposed component may contain multiple signals erroneously. Although the optimization of α will be an important task in future work, such an optimization lies outside the scope of this study.

TABLE 11. Performance for different values of VME parameter α.

Evaluation index	Method	VME parameter α 1,000	10,000	30,000	100,000	300,000
RMSE (ms)	C3	34.68	62.27	–	47.37	43.50
	C4	34.68	62.27	–	39.36	36.73
	P3	23.20	31.47	48.95	41.63	45.53
	P4	23.24	26.82	24.86	21.76	31.39
CC	C3	0.57	-0.12	–	0.28	0.43
	C4	0.57	-0.12	–	0.38	0.50
	P3	0.83	0.68	0.46	0.58	0.66
	P4	0.83	0.81	0.80	0.83	0.68
TCR (%)	C3	37.04	10.46	0	48.61	73.87
	C4	37.04	10.46	0	55.52	78.89
	P3	82.23	79.55	61.78	78.71	71.21
	P4	82.23	90.18	88.92	91.63	83.07

E. COMPARISON WITH RELATED WORKS

Next, we compare the proposed method with several other existing methods, which have been classified into four categories: spectrum-based, periodicity-based, mix source separation-based, and deep-learning-based methods [27]. Among these categories, deep learning-based methods have emerged as a particularly active research area in recent years. Toda et al. [51] proposed a method that combined a convolutional neural network (CNN) with first-order differentiation-based preprocessing. Wu et al. [52] proposed a model that incorporated a self-attention-based separator into an encoder-decoder architecture to allow simultaneous reconstruction of ECG and respiration signals. Table 12 shows the error values reported for radar-based IBI estimation in related articles. Although some of the previous works [1], [52] have reported higher accuracies than those reported in this study, the proposed method achieves relatively high accuracy, even in comparison to some of the most recent research articles.

For comparison, we applied the deep learning-based method proposed by Chang et al. [53] to our data set, where we set the time window length at 6.0 s. In this performance evaluation, the leave-one-out cross-validation approach was used for 25 datasets. Performance results are summarized in Table 12. Compared with the method of Chang et al. [53], the proposed method provides better performance in terms of all metrics (RMSE, CC, and TCR). In [53], the mean absolute error (MAE) for the heart rate (HR) was reported to be 2.88 bpm, which is equivalent to an IBI error of 27 ms if the heart rate is assumed to be 80 bpm. In contrast, when the conventional method was applied to our data set, the IBI estimation error was 96.55 ms, indicating a clear accuracy degradation. This discrepancy can be explained by the differences in the size of the data set used for training; the previous study [53] used data from only three participants, with a total recording time of 81 min, while our data set included data acquired from eleven participants with a total recording time of 25 min. This indicates that the proposed method is capable of accurate HR estimation, even when a large data set cannot be prepared.

TABLE 12. Comparison with related works.

	Deep learning-based	IBI error (ms)	CC	TCR (%)
Petrovic et al. [1]	-	16.70	-	-
Wang et al. [16]	-	28.00	-	-
Yamamoto et al. [50]	-	47.50	-	-
Yamamoto et al. [14]	✓	111.00	-	-
Toda et al. [51]	✓	102.20	-	-
Wu et al. [52]	✓	2.50	-	-
Chang et al. [53]	✓	96.55	0.00	32.00
This work (P4)	-	26.02	0.74	88.27

F. OVERALL DISCUSSION

In this section, we explain why the proposed method can effectively eliminate the harmonic influence of the respiration. First, the second derivative acts as a high-pass filter that emphasizes the harmonic components of the heartbeat along with the high-frequency noise and the harmonics of the respiration. Next, the VME specifically extracts the second harmonic component of the heartbeat while suppressing all other components because the desired frequency ω_{d} can be specified in the VME algorithm; this approach works as long as the harmonic components of the respiration do not coincide exactly with the second harmonic component of the heartbeat.

In this study, the participants were instructed to remain stationary and breathe normally during the radar measurements. However, in normal daily environments, it is natural for people to make body movements that affect the radar measurements. In these cases, the HR cannot be estimated accurately, even when using our proposed method. Therefore, it will be an important task to develop a method that can accurately estimate the HR when the subject's body movements cannot be ignored.

In the measurements performed during this study, the radar measurements were performed for each participant individually, rather than for all participants simultaneously. When multiple individuals are measured at the same time, the resulting interference makes it difficult to extract the respiration and heartbeat signals from each person. Therefore, separating the vital sign signals of each individual becomes an essential step [54], [55]. Ahmad et al. [56] used spatial information obtained through a combination of range-gating and beamforming to separate signals from multiple individuals. Xu et al. [57] performed simultaneous monitoring of multiple subjects by controlling the transmission beams of a time-division multiplexing phase array radar system. Liu et al. [58] applied a resonance-based sparse separation algorithm to estimate the respiratory and heart rates of multiple individuals located within the same range bin. The proposed method is compatible with signal separation techniques of this type based on the spatial information obtained via adaptive array signal processing and it holds the potential to perform efficient extraction of heartbeat signals even in multi-subject scenarios. Despite this consideration, this approach lies outside the scope of the current study, although it will provide an important research topic for future projects.

In this study, we used a radar system with an operating frequency band of 77–81 GHz. The proposed method was not designed specifically for this frequency band. Therefore, the proposed method is also expected to be applied to radar systems with different operating frequency bands. However, it will be important to investigate the applicability of our proposed method to different types of radar systems with various operating frequency bands.

In this study, we evaluated the performance of the proposed method for eleven participants. However, the participants were all men in their 20s, which serves to illustrate the potential limitations of this study associated with the sample sizes and the diversity of the group of participants. Therefore, it will be important to conduct additional large-scale measurements to ensure diversity in terms of the age, sex, and health conditions of all participants in our future work.

From a practical viewpoint, the proposed method will be integrated into an existing radar-based vital sign monitoring system called VitaWatcher (MaRI Company Ltd., Kyoto) that was developed in part by one of the authors (Prof. Sakamoto). This integration is achievable because the proposed method can be implemented simply by updating the existing system's software.

VI. CONCLUSION

In this study, we have proposed a radar-based method for the estimation of heart IBIs that uses a combination of the absolute value of the second derivative of the complex radar signal and the VME method. Unlike many conventional methods, the proposed method does not estimate a body displacement waveform that is proportional to the phase of the complex radar signal. We have demonstrated that the heartbeat components were amplified effectively when using the second-derivative-based approach, which was emphasized selectively by the VME method, with a resultant improvement in accuracy when estimating the heart IBI. By performing measurements on eleven participants using a 79 GHz array radar system, the proposed method was shown to be able to estimate their heart IBIs using the topology method; this approach improved the average correlation coefficient of the actual and estimated IBIs by 0.2 and it also reduced the average RMSE by 23%. The proposed method is expected to make a significant contribution to the development of practical noncontact medical and healthcare monitoring systems. Our next step in this work will be to evaluate the performance of the proposed method when using large-scale data acquired from a larger number of participants with diversity in terms of their age, gender, and health conditions. It will also be important to study the possibility of combining the proposed radar-based system with other types of noncontact sensors, including optical cameras, laser sensors, and ultrasonic sensors.

ACKNOWLEDGMENT

The authors thank Li-An Yang of Kyoto University for analyzing the acquired data using machine learning algorithms and they also thank Dr. Hirofumi Taki and Dr. Shigeaki Okumura of MaRI Company Ltd., for providing technical advice. They also thank all parties involved for their cooperation in conducting this research. They thank David MacDonald, M.Sc., from Edanz (https://jp.edanz.com/ac) for editing a draft of this manuscript.

REFERENCES

[1] V. L. Petrović, M. M. Janković, A. V. Lupšić, V. R. Mihajlovic, and J. S. Popovic-Božovic, "High-accuracy real-time monitoring of heart rate variability using 24 GHz continuous-wave Doppler radar," *IEEE Access*, vol. 7, pp. 74721–74733, 2019, doi: 10.1109/ACCESS.2019.2921240.

[2] Z. Chen, Y. Liu, C. Sui, M. Zhou, and Y. Song, "A novel scheme for suppression of human motion effects in non-contact heart rate detection," *IEEE Access*, vol. 11, pp. 84241–84257, 2023, doi: 10.1109/ACCESS.2023.3302918.

[3] Z. Yue, S. Ding, S. Yang, L. Wang, and Y. Li, "Multimodal information fusion approach for noncontact heart rate estimation using facial videos and graph convolutional network," *IEEE Trans. Instrum. Meas.*, vol. 71, pp. 1–13, 2022, doi: 10.1109/TIM.2021.3129498.

[4] B. R. Upadhyay, A. B. Baral, and M. Torlak, "Vital sign detection via angular and range measurements with mmWave MIMO radars: Algorithms and trials," *IEEE Access*, vol. 10, pp. 106017–106032, 2022, doi: 10.1109/ACCESS.2022.3211527.

[5] H. Wang, F. Du, H. Zhu, Z. Zhang, Y. Wang, Q. Cao, and X. Zhu, "HeRe: Heartbeat signal reconstruction for low-power millimeter-wave radar based on deep learning," *IEEE Trans. Instrum. Meas.*, vol. 72, pp. 1–15, 2023, doi: 10.1109/TIM.2023.3267348.

[6] L. Liu, J. Zhang, Y. Qu, S. Zhang, and W. Xiao, "MmRH: Noncontact vital sign detection with an FMCW mm-wave radar," *IEEE Sensors J.*, vol. 23, no. 8, pp. 8856–8866, Apr. 2023, doi: 10.1109/JSEN.2023.3250500.

[7] D. Obeid, S. Sadek, G. Zaharia, and G. El Zein, "Multitunable microwave system for touchless heartbeat detection and heart rate variability extraction," *Microw. Opt. Technol. Lett.*, vol. 52, no. 1, pp. 192–198, Jan. 2010, doi: 10.1002/mop.24877.

[8] J. Kranjec, S. Beguš, G. Geršak, and J. Drnovšek, "Non-contact heart rate and heart rate variability measurements: A review," *Biomed. Signal Process. Control*, vol. 13, pp. 102–112, Sep. 2014, doi: 10.1016/j.bspc.2014.03.004.

[9] D. H. Spodick, "Survey of selected cardiologists for an operational definition of normal sinus heart rate," *Amer. J. Cardiology*, vol. 72, no. 5, pp. 487–488, Aug. 1993, doi: 10.1016/0002-9149(93)91153-9.

[10] M. Le and B. Van Nguyen, "Multivariate correlation of higher harmonics for heart rate remote measurement using UWB impulse radar," *IEEE Sensors J.*, vol. 20, no. 4, pp. 1859–1866, Feb. 2020, doi: 10.1109/JSEN.2019.2950635.

[11] Y. Rong and D. W. Bliss, "Remote sensing for vital information based on spectral-domain harmonic signatures," *IEEE Trans. Aerosp. Electron. Syst.*, vol. 55, no. 6, pp. 3454–3465, Dec. 2019, doi: 10.1109/TAES.2019.2917489.

[12] M. Nosrati and N. Tavassolian, "Accurate Doppler radar-based cardiopulmonary sensing using chest-wall acceleration," *IEEE J. Electromagn., RF Microw. Med. Biol.*, vol. 3, no. 1, pp. 41–47, Mar. 2019, doi: 10.1109/JERM.2018.2879452.

[13] S. Hochreiter and J. Schmidhuber, "Long short-term memory," *Neural Comput.*, vol. 9, no. 8, pp. 1735–1780, Nov. 1997, doi: 10.1162/neco.1997.9.8.1735.

[14] K. Yamamoto and T. Ohtsuki, "Non-contact heartbeat detection by heartbeat signal reconstruction based on spectrogram analysis with convolutional LSTM," *IEEE Access*, vol. 8, pp. 123603–123613, 2020, doi: 10.1109/ACCESS.2020.3006107.

[15] F. Wang, X. Zeng, C. Wu, B. Wang, and K. J. R. Liu, "MmHRV: Contactless heart rate variability monitoring using millimeter-wave radio," *IEEE Internet Things J.*, vol. 8, no. 22, pp. 16623–16636, Nov. 2021, doi: 10.1109/JIOT.2021.3075167.

[16] K. Dragomiretskiy and D. Zosso, "Variational mode decomposition," *IEEE Trans. Signal Process.*, vol. 62, no. 3, pp. 531–544, Feb. 2014, doi: 10.1109/TSP.2013.2288675.

[17] G. Beltrão, W. A. Martins, B. Shankar M. R., M. Alaee-Kerahroodi, U. Schroeder, and D. Tatarinov, "Adaptive nonlinear least squares framework for contactless vital sign monitoring," *IEEE Trans. Microw. Theory Techn.*, vol. 71, no. 4, pp. 1696–1710, Apr. 2023, doi: 10.1109/TMTT.2022.3222384.

[18] P. Zheng, C. Zheng, X. Li, H. Chen, A. Wang, and Y. Luo, "Second harmonic weighted reconstruction for non-contact monitoring heart rate," *IEEE Sensors J.*, vol. 22, no. 6, pp. 5815–5823, Mar. 2022, doi: 10.1109/JSEN.2022.3148003.

[19] I. Iwata, T. Sakamoto, T. Matsumoto, and S. Hirata, "Noncontact measurement of heartbeat of humans and chimpanzees using millimeter-wave radar with topology method," *IEEE Sensors Lett.*, vol. 7, no. 11, pp. 1–4, Nov. 2023, doi: 10.1109/LSENS.2023.3322287.

[20] I. Kakouche, M. S. Azzaz, A. Maali, and A. Mesloub, "New measurement method for respiration and heartbeat estimation using IR-UWB radar," in *Proc. 6th Int. Conf. Image Signal Process. Appl. (ISPA)*, Mostaganem, Algeria, Nov. 2019, pp. 1–6, doi: 10.1109/ISPA48434.2019.8966792.

[21] H. T. Yen, M. Kurosawa, T. Kirimoto, Y. Hakozaki, T. Matsui, and G. Sun, "Non-contact estimation of cardiac inter-beat interval and heart rate variability using time-frequency domain analysis for CW radar," *IEEE J. Electromagn., RF Microw. Med. Biol.*, vol. 7, no. 4, pp. 457–467, Dec. 2023, doi: 10.1109/JERM.2023.3326562.

[22] Y. Xiong, Z. Peng, C. Gu, S. Li, D. Wang, and W. Zhang, "Differential enhancement method for robust and accurate heart rate monitoring via microwave vital sign sensing," *IEEE Trans. Instrum. Meas.*, vol. 69, no. 9, pp. 7108–7118, Sep. 2020, doi: 10.1109/TIM.2020.2978347.

[23] S. Ji, H. Wen, J. Wu, Z. Zhang, and K. Zhao, "Systematic heartbeat monitoring using a FMCW mm-wave radar," in *Proc. IEEE Int. Conf. Consum. Electron. Comput. Eng. (ICCECE)*, Guangzhou, China, Jan. 2021, pp. 714–718, doi: 10.1109/ICCECE51280.2021.9342280.

[24] T. Sakamoto and R. Yamaguchi, "A method of estimating accuracy in noncontact measurement of heart rate using millimeter-wave radar," in *Proc. IEICE*, 2019, pp. 1–12.

[25] I. Iwata, K. Sumi, Y. Tanaka, and T. Sakamoto, "Accurate radar-based heartbeat measurement using higher harmonic components," 2024, *arXiv:2407.07380*.

[26] Y. Wu, H. Ni, C. Mao, J. Han, and W. Xu, "Non-intrusive human vital sign detection using mmWave sensing technologies: A review," *ACM Trans. Sensor Netw.*, vol. 20, no. 1, pp. 1–36, Nov. 2023, doi: 10.1145/3627161.

[27] Y. Zhang, R. Yang, Y. Yue, E. G. Lim, and Z. Wang, "An overview of algorithms for contactless cardiac feature extraction from radar signals: Advances and challenges," *IEEE Trans. Instrum. Meas.*, vol. 72, pp. 1–20, 2023, doi: 10.1109/TIM.2023.3300471.

[28] Y. Yin, X. Yu, H. Lv, M. Liu, F. Qi, and J. Wang, "Micro-vibration distinguishment between humans and animals based on ensemble empirical mode decomposition using ultra-wide band radar," *J. Eng.*, vol. 2019, no. 21, pp. 7469–7472, Sep. 2019, doi: 10.1049/joe.2019.0619.

[29] Z. Hao, H. Yan, X. Dang, Z. Ma, W. Ke, and P. Jin, "RMVS: Remote monitoring of vital signs with mm-wave radar," in *Proc. 1st ACM Workshop AI Empowered Mobile Wireless Sens.*, New York, NY, USA, Oct. 2022, pp. 1–6, doi: 10.1145/3556558.3558578.

[30] W. Hu, Z. Zhao, Y. Wang, H. Zhang, and F. Lin, "Noncontact accurate measurement of cardiopulmonary activity using a compact quadrature Doppler radar sensor," *IEEE Trans. Biomed. Eng.*, vol. 61, no. 3, pp. 725–735, Mar. 2014, doi: 10.1109/TBME.2013.2288319.

[31] L. Sun, S. Huang, Y. Li, C. Gu, H. Pan, H. Hong, and X. Zhu, "Remote measurement of human vital signs based on joint-range adaptive EEMD," *IEEE Access*, vol. 8, pp. 68514–68524, 2020, doi: 10.1109/ACCESS.2020.2985286.

[32] C. Zhao, W. Zeng, D. Hu, and H. Liu, "Robust heart rate monitoring by a single wrist-worn accelerometer based on signal decomposition," *IEEE Sensors J.*, vol. 21, no. 14, pp. 15962–15971, Jul. 2021, doi: 10.1109/JSEN.2021.3075109.

[33] Y. Wang, R. Markert, J. Xiang, and W. Zheng, "Research on variational mode decomposition and its application in detecting rub-impact fault of the rotor system," *Mech. Syst. Signal Process.*, vols. 60–61, pp. 243–251, Aug. 2015, doi: 10.1016/j.ymssp.2015.02.020.

[34] K. Adamczyk and A. G. Polak, "Derivation of frequency components from overnight heart rate variability using an adaptive variational mode decomposition," in *Proc. 43rd Annu. Int. Conf. IEEE Eng. Med. Biol. Soc. (EMBC)*, Nov. 2021, pp. 647–650, doi: 10.1109/EMBC46164.2021.9630414.

[35] P. Wang, Y. Ma, F. Liang, Y. Zhang, X. Yu, Z. Li, Q. An, H. Lv, and J. Wang, "Non-contact vital signs monitoring of dog and cat using a UWB radar," *Animals*, vol. 10, no. 2, p. 205, Jan. 2020, doi: 10.3390/ani10020205.

[36] J. Zhao, X. Chen, X. Zhang, and X. Chen, "A solution for co-frequency and low SNR problems in heart rate estimation based on photoplethysmography signals," *Med. Biol. Eng. Comput.*, vol. 60, no. 12, pp. 3419–3433, Oct. 2022, doi: 10.1007/s11517-022-02678-x.

[37] Q. Lele, L. Shujie, G. Wenwen, M. Shuang, and Y. Tianhong, "Vital sign detection using multichannel FMCW radar," in *Proc. CIE Int. Conf. Radar (Radar)*, Hainan, China, Dec. 2021, pp. 3027–3030, doi: 10.1109/Radar53847.2021.10028620.

[38] W. Huang, R. Wang, Y. Zhuang, Z. Wang, and Q. Du, "Adaptive harmonic detection of active power filter based on improved VMD," in *Proc. IEEE 5th Int. Electr. Energy Conf. (CIEEC)*, Nangjing, China, May 2022, pp. 2682–2686, doi: 10.1109/CIEEC54735.2022.9845851.

[39] M. Nazari and S. M. Sakhaei, "Variational mode extraction: A new efficient method to derive respiratory signals from ECG," *IEEE J. Biomed. Health Informat.*, vol. 22, no. 4, pp. 1059–1067, Jul. 2018, doi: 10.1109/JBHI.2017.2734074.

[40] Y. Zhang, G. Jin, Y. Liu, Z. Chen, Y. Song, and H. Li, "A new heart rate detection scheme based on genetic algorithm for VME parameter optimization," in *Proc. Int. Seminar Comput. Sci. Eng. Technol.*, Apr. 2023, pp. 767–771, doi: 10.1109/scset58950.2023.00172.

[41] M. A. Colominas, G. Schlotthauer, and M. E. Torres, "Improved complete ensemble EMD: A suitable tool for biomedical signal processing," *Biomed. Signal Process. Control*, vol. 14, pp. 19–29, Nov. 2014, doi: 10.1016/j.bspc.2014.06.009.

[42] G. Paterniani, D. Sgreccia, A. Davoli, G. Guerzoni, P. Di Viesti, A. C. Valenti, M. Vitolo, G. M. Vitetta, and G. Boriani, "Radar-based monitoring of vital signs: A tutorial overview," *Proc. IEEE*, vol. 111, no. 3, pp. 277–317, Mar. 2023, doi: 10.1109/JPROC.2023.3244362.

[43] F.-K. Wang, J.-X. Zhong, and J.-Y. Shih, "IQ signal demodulation for noncontact vital sign monitoring using a CW Doppler radar: A review," *IEEE J. Electromagn., RF Microw. Med. Biol.*, vol. 6, no. 4, pp. 449–460, Dec. 2022, doi: 10.1109/JERM.2022.3214753.

[44] Y. Zhao, Y. Liu, and Z. Cai, "A novel scheme for vital sign detection with FMCW radar," in *Proc. Global Rel. Prognostics Health Manage. (PHM-Yantai)*, Yantai, China, Oct. 2022, pp. 1–6, doi: 10.1109/PHM-Yantai55411.2022.9942085.

[45] Y. Hu and T. Toda, "Remote vital signs measurement of indoor walking persons using mm-wave FMCW radar," *IEEE Access*, vol. 10, pp. 78219–78230, 2022, doi: 10.1109/ACCESS.2022.3193789.

[46] Z. Yang and Z. Bao, "Short-time heart rate estimation based on 60-GHz FMCW radar," in *IEEE MTT-S Int. Microw. Symp. Dig.*, Qingdao, China, May 2023, pp. 1–3, doi: 10.1109/iws58240.2023.10222194.

[47] A. Hyvarinen, "Fast and robust fixed-point algorithms for independent component analysis," *IEEE Trans. Neural Netw.*, vol. 10, no. 3, pp. 626–634, May 1999, doi: 10.1109/72.761722.

[48] T. Sakamoto, R. Imasaka, H. Taki, T. Sato, M. Yoshioka, K. Inoue, T. Fukuda, and H. Sakai, "Feature-based correlation and topological similarity for interbeat interval estimation using ultrawideband radar," *IEEE Trans. Biomed. Eng.*, vol. 63, no. 4, pp. 747–757, Apr. 2016, doi: 10.1109/TBME.2015.2470077.

[49] T. Sakamoto, S. Mitani, and T. Sato, "Noncontact monitoring of heartbeat and movements during sleep using a pair of millimeter-wave ultra-wideband radar systems," *IEICE Trans. Commun.*, vol. E104.B, no. 4, pp. 463–471, Apr. 2021, doi: 10.1587/transcom.2020ebp3078.

[50] K. Yamamoto, K. Toyoda, and T. Ohtsuki, "Spectrogram-based non-contact RRI estimation by accurate peak detection algorithm," *IEEE Access*, vol. 6, pp. 60369–60379, 2018, doi: 10.1109/ACCESS.2018.2875737.

[51] D. Toda, R. Anzai, K. Ichige, R. Saito, and D. Ueki, "ECG signal reconstruction using FMCW radar and a convolutional neural network for contactless vital-sign sensing," *IEICE Trans. Commun.*, vol. 106, no. 1, pp. 65–73, Jun. 2022, doi: 10.1587/transcom.2022ebp3005.

[52] Y. Wu, H. Ni, C. Mao, and J. Han, "Contactless reconstruction of ECG and respiration signals with mmWave radar based on RSSRnet," *IEEE Sensors J.*, vol. 24, no. 5, pp. 6358–6368, Mar. 2024, doi: 10.1109/JSEN.2023.3333025.

[53] H.-Y. Chang, C.-H. Hsu, and W.-H. Chung, "Fast acquisition and accurate vital sign estimation with deep learning-aided weighted scheme using FMCW radar," in *Proc. IEEE 95th Veh. Technol. Conf., (VTC-Spring)*, Helsinki, Finland, Jun. 2022, pp. 1–6, doi: 10.1109/VTC2022-Spring54318.2022.9860799.

[54] Y. Liu, X.-G. Xia, H. Liu, A. H. T. Nguyen, and A. W. H. Khong, "Iterative implementation method for robust target localization in a mixed interference environment," *IEEE Trans. Geosci. Remote Sens.*, vol. 60, 2022, Art. no. 5107813, doi: 10.1109/TGRS.2021.3131327.

[55] S. M. M. Islam, E. Yavari, A. Rahman, V. M. Lubecke, and O. Boric-Lubecke, "Direction of arrival estimation of physiological signals of multiple subjects using phase comparison monopulse radar," in *Proc. Asia–Pacific Microw. Conf. (APMC)*, Kyoto, Japan, Nov. 2018, pp. 411–413, doi: 10.23919/APMC.2018.8617539.

[56] A. Ahmad, J. C. Roh, D. Wang, and A. Dubey, "Vital signs monitoring of multiple people using a FMCW millimeter-wave sensor," in *Proc. IEEE Radar Conf. (RadarConf)*, Oklahoma City, OK, USA, Apr. 2018, pp. 1450–1455, doi: 10.1109/RADAR.2018.8378778.

[57] Z. Xu, C. Shi, T. Zhang, S. Li, Y. Yuan, C. M. Wu, Y. Chen, and A. Petropulu, "Simultaneous monitoring of multiple People's vital sign leveraging a single phased-MIMO radar," *IEEE J. Electromagn., RF Microw. Med. Biol.*, vol. 6, no. 3, pp. 311–320, Sep. 2022, doi: 10.1109/JERM.2022.3143431.

[58] Y. Liu, X. Fu, R. C. Tewari, X. Wang, and A. W. H. Khong, "Contactless vital sign monitoring for multiple people using a millimeter-wave MIMO radar," in *Proc. IEEE Int. Conf. Acoust., Speech Signal Process. (ICASSP)*, Hyderabad, India, Apr. 2025, pp. 1–5, doi: 10.1109/icassp49660.2025.10890100.

ITSUKI IWATA received the B.E. and M.E. degrees from Kyoto University, Kyoto, Japan, in 2022 and 2024, respectively. He was a recipient of the IEEE Antennas and Propagation Society Kansai Joint Chapter Young Engineer Technical Meeting Best Presentation Award, in 2021.

KIMITAKA SUMI (Graduate Student Member, IEEE) received the B.E. and M.E. degrees from Nagoya University, Aichi, Japan, in 2020 and 2022, respectively. He is currently pursuing the Ph.D. degree with the Graduate School of Engineering, Kyoto University. His research interests include signal processing and remote sensing.

YUJI TANAKA (Member, IEEE) received the B.E., M.E., and Ph.D. degrees in engineering from Kanazawa University, Ishikawa, Japan, in 2015, 2017, and 2023, respectively. From 2017 to 2020, he was with the Information Technology Research and Development Center, Mitsubishi Electric Corporation. From 2023 to 2024, he was an Assistant Professor with the Graduate School of Engineering, Kyoto University. He is currently an Assistant Professor with the Graduate School of Engineering, Nagoya Institute of Technology. His research interests include radar signal processing, radio science, and radar measurement of physiological signals. He is a member of the Institute of Electronics, Information and Communication Engineers (IEICE); and the Society of Geomagnetism and Earth, Planetary and Space Sciences (SGEPSS). He received the Second Prize in the URSI-JRSM 2022 Student Paper Competition and the Young Researcher's Award from IEICE Technical Committee on Electronics Simulation Technology.

TAKUYA SAKAMOTO (Senior Member, IEEE) received the B.E. degree in electrical and electronic engineering from Kyoto University, Kyoto, Japan, in 2000, and the M.I. and Ph.D. degrees in communications and computer engineering from the Graduate School of Informatics, Kyoto University, in 2002 and 2005, respectively.

From 2006 to 2015, he was an Assistant Professor with the Graduate School of Informatics, Kyoto University. From 2011 to 2013, he was also a Visiting Researcher with Delft University of Technology, Delft, The Netherlands. From 2015 to 2019, he was an Associate Professor with the Graduate School of Engineering, University of Hyogo, Himeji, Japan. In 2017, he was also a Visiting Scholar with the University of Hawaii at Manoa, Honolulu, HI, USA. From 2019 to 2022, he was an Associate Professor with the Graduate School of Engineering, Kyoto University. From 2018 to 2022, he was also a PRESTO Researcher with Japan Science and Technology Agency, Japan. Since 2022, he has been a Professor with the Graduate School of Engineering, Kyoto University. His current research interests include wireless human sensing, radar signal processing, and radar measurement of physiological signals. He was a recipient of the Best Paper Award from the International Symposium on Antennas and Propagation (ISAP), in 2004; the Young Researcher's Award from the Institute of Electronics, Information and Communication Engineers of Japan (IEICE), in 2007; the Best Presentation Award from the Institute of Electrical Engineers of Japan, in 2007; the Best Paper Award from the ISAP, in 2012; the Achievement Award from the IEICE Communications Society, in 2015, 2018, and 2023; the Achievement Award from the IEICE Electronics Society, in 2019; the Masao Horiba Award, in 2016; the Best Presentation Award from the IEICE Technical Committee on Electronics Simulation Technology, in 2022; the Telecom System Technology Award from the Telecommunications Advancement Foundation, in 2022; and the Best Paper Award from the IEICE Communication Society, in 2007 and 2023.